Physics of Fluids

Numerical investigations of head-on collisions of binary unequal-sized droplets on superhydrophobic walls

Cite as: Phys. Fluids **33**, 032001 (2021); https://doi.org/10.1063/5.0038352
Submitted: 30 November 2020 . Accepted: 13 January 2021 . Published Online: 03 March 2021

Yongpan Cheng (程永攀), Jiwei Li (李季巍), Jinliang Xu (徐进良), and Yang Shen (沈阳)

COLLECTIONS

This paper was selected as an Editor's Pick

View Online Export Citation CrossMark

Physics of Fluids GALLERY OF COVERS

AIP Publishing

© 2021 Author(s).

Physics of Fluids ARTICLE scitation.org/journal/phf

Numerical investigations of head-on collisions of binary unequal-sized droplets on superhydrophobic walls

Cite as: Phys. Fluids 33, 032001 (2021); doi: 10.1063/5.0038352
Submitted: 30 November 2020 · Accepted: 13 January 2021 ·
Published Online: 3 March 2021

View Online Export Citation CrossMark

Yongpan Cheng (程永攀),[1,2] Jiwei Li (李季巍),[1] Jinliang Xu (徐进良),[1,2,a)] and Yang Shen (沈阳)[1]

AFFILIATIONS

[1]Beijing Key Laboratory of Multiphase Flow and Heat Transfer for Low Grade Energy, North China Electric Power University, Beijing 102206, China
[2]Key Laboratory of Power Station Energy Transfer Conversion and System of Ministry of Education, North China Electric Power University, Beijing 102206, China

[a)]Author to whom correspondence should be addressed: xjl@ncepu.edu.cn

ABSTRACT

Droplet head-on impact is widely encountered in nature, industry, and agricultural applications. In our study, a two-dimensional axisymmetric model, using the volume-of-fluid method, is built to simulate unequally sized droplet head-on impact on a superhydrophobic surface. The collision regime, after droplet coalescence, is obtained with dimensionless parameters, as well as the contact time, maximum spreading diameter, restitution coefficient, and viscous dissipation. When the impact droplet is larger than the stationary droplet on the substrate, the merged droplet can easily jump up. At high Bond numbers (*Bo*) or high Ohnesorge numbers (*Oh*), the merged droplet cannot jump up due to significant gravitational effects or viscous effects, respectively. The energy for droplet jumping mainly comes from the released surface energy after the coalescence of father and mother droplets. The contact time of a droplet with the superhydrophobic substrate is proportional to the Weber number to the 0.5th power ($We^{0.5}$), and the maximum spreading diameter of a merged droplet is proportional to $We^{0.2}$. With an increasing size ratio of the father droplet to the mother droplet, both the contact time and maximum spreading diameter increase. These findings will help gain insights into the dynamics of droplet head-on impact.

Published under license by AIP Publishing. https://doi.org/10.1063/5.0038352

I. INTRODUCTION

Droplet head-on collision is a typical phenomenon in nature, found in, for example, rain drop formation and falling;[1,2] it also enjoys wide application in industry and agriculture, in, for example, inkjet printing,[3] spray drying,[4] and fuel combustion.[5,6] In inkjet printing,[7] in order to obtain high-quality, continuous, printed lines, the incoming impact droplet must overlap and coalesce with the settled droplet without jet formation. In aircraft-ice removal,[8] to avoid water accumulation on the aircraft surface, surface droplets are removed by droplet impact on sessile drops. By controlling the coalescence and rebound of collision droplets, Boolean operations can be realized for information technology.[9]

Droplet collision is affected by several parameters, such as droplet impact velocity, droplet size, liquid properties, and substrate wettability. By adjusting these parameters, the collision dynamics can be controlled; hence, the collision regime is crucial for specific applications of droplet collisions. Jiang *et al.*[10] experimentally studied the collisions of water and hydrocarbon droplets of equal size and found that, depending on the impact Weber number, the collisions might enter coalescence, bouncing, or separation regimes. Qian and Law[11] extended the study by changing atmospheric pressure and gas properties and found that five distinct collision regimes existed for droplet head-on collisions under free flying conditions in terms of their coalescence, bouncing, and separation. Willis and Orme[12] studied droplet collisions in vacuum, without aerodynamic effects, and found that the Weber number describing the regime boundary changed greatly compared with collisions at standard atmospheric pressure. Wang *et al.*[13] experimentally studied the head-on collisions of binary droplets at low velocity and found four different regimes in terms of complete or partial rebound or coalescence. The contact time for complete rebound was 10 ms–20 ms, which is predicted accurately using Hertz contact theory.

Published under license by AIP Publishing

Compared with equally sized droplet collisions, unequally sized droplet collisions are more widely encountered. Brazier-Smith *et al.*[14] studied unequally sized water droplet collisions and showed the effect of the impact parameter on the boundary of the coalescence regime and separation regime. Ashgriz and Poo[15] conducted similar experiments and obtained the transition Weber number for the coalescence regime to the separation regime. By including the size ratio in a symmetric Weber number, Rabe *et al.*[16] derived a formula to describe the transition regimes of unequally sized droplet collisions, which agreed well with their experimental data. Tang *et al.*[17] studied the head-on collisions of water and hydrocarbon droplets of unequal size, showing that the collision regime is a function of size ratio and collision Weber number; they also showed the effect of the size ratio on the transition Weber number in the regimes. Zhang *et al.*[18] experimentally found that unequally sized droplet collisions promote the formation of satellite droplets and that the critical size ratio for satellite droplet formation depended on the Ohnesorge number (*Oh*). Yi *et al.*[19] studied the head-on collisions of droplets at different temperatures on a superhydrophobic surface and found that increasing temperature promoted droplet coalescence after collisions.

As droplet collisions involve multiple time scales and length scales, some details cannot be easily observed experimentally. On the contrary, numerical simulation provides a feasible way to gain insights into droplet dynamics. Sakakibara and Inamuro[20] simulated unequally sized droplet collisions using the lattice Boltzmann method (LBM). The boundaries between the droplet-coalescence and separation regimes agreed well with available theoretical predictions. Premnath and Abraham[21] also adopted LBM to simulate head-on and off-center droplet collisions and found that at high-impact Weber numbers, reflexive separation occurred with or without satellite droplet formation. A high Weber number tended to increase the satellite-droplet size, while the Ohnesorge number tended to decrease the satellite-droplet size. Nikolopoulos and Bergeles[22] investigated the central collisions of unequally sized droplets with different droplet-size ratios, as well as gas and liquid properties using the volume-of-fluid method; they also investigated the mixing process after droplet coalescence by using a color function. Using a front-tracking method, Liu *et al.*[23] found that unequally sized droplet collisions promoted mixing compared with equally sized droplet collisions. Graham *et al.*[24] studied droplet collisions with varying wettability, incoming velocity, and droplet size. They found that the maximum spreading length decreased with increasing hydrophobicity.

From the literature review above, it can be seen that most of the studies are focused on the collision between two suspended droplets in the air with equal sizes or unequal sizes;[6,10,11,15–17,22] only a limited number of studies focus on the droplet collisions on a substrate.[8,9,24] The regimes are still not clear whether the collision droplet can jump up from the substrate or not, as well as the underlying mechanism for droplet dynamics. Furthermore, for head-on collision of binary droplets on a substrate, surface wettability, liquid viscosity, impact dynamics, droplet gravity, the droplet size, and the size ratio all significantly affect droplet collisions. After droplet collision, coalescence, bouncing, splashing, and breakup may occur, the dynamics of which need to be investigated in detail.

In this paper, a numerical model is built to study head-on droplet collisions. After model validation using reliable experimental data, the model simulates droplet collisions on a superhydrophobic surface. Then, the collision regimes are provided under different size ratios, Bond numbers (*Bo*), Weber numbers, and Ohnesorge numbers; the dynamics of each region are analyzed in detail. Finally, conclusions are drawn for unequally sized droplet collisions, which will provide guidelines for the application of such in various fields.

II. NUMERICAL SIMULATION

A. Physical model

Figure 1 shows a collision between two droplets of different size on a superhydrophobic surface. The father droplet is stationary, and the mother droplet falls down toward the center, colliding with the father droplet in the vertical direction. Coalescence, bounce, and breakup may occur, depending on interactions involving inertial force, capillary force, and gravitational force during collision.

B. Governing equations

Due to the axisymmetric characteristics of droplet head-on collision, for simplification, a two-dimensional, cylindrical coordinate system (r, z) is adopted to simulate droplet dynamics, and the volume-of-fluid method is used to simulate the evolution of the gas–liquid

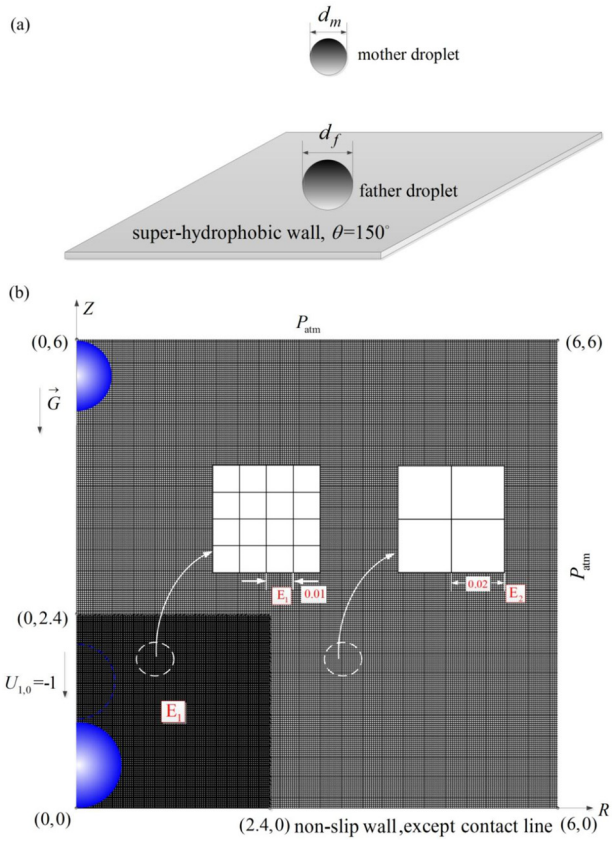

FIG. 1. Head-on collision of an unequally sized droplet on a super-hydrophobic surface. (a) Schematic diagram. (b) Grid system.

Published under license by AIP Publishing

surface. The initial diameters of the mother droplet and father droplet are d_m and d_f, respectively, the size ratio is $a_i = d_f/d_m$, and the velocity of the mother droplet is $u_{m,0}$. With d_m and $u_{m,0}$ as the characteristic length and velocity, respectively, and the liquid properties as the reference values, the following dimensionless parameters are defined:

$$\text{Reynolds number} \quad Re = \frac{\rho_l u_{m,0} d_m}{\mu_l}, \tag{1a}$$

$$\text{Weber number} \quad We = \frac{\rho_l u_{m,0}^2 d_m}{\sigma}, \tag{1b}$$

$$\text{Dimensionless pressure} \quad P = \frac{p}{\rho_l u_{m,0}^2}, \tag{1c}$$

$$\text{Dimensionless gravity} \quad G = \frac{g d_m}{u_{m,0}^2}, \tag{1d}$$

$$\text{Dimensionless density} \quad \Theta = \frac{\rho}{\rho_l}, \tag{1e}$$

$$\text{Dimensionless viscosity} \quad \Upsilon = \frac{\mu}{\mu_l}. \tag{1f}$$

Thus, the non-dimensional governing equations are as follows:

Continuity equation:

$$\nabla \cdot \vec{V} = 0, \tag{2}$$

Momentum equation:

$$\frac{\partial \vec{V}}{\partial \tau} + \vec{V} \cdot \nabla \vec{V} = -\frac{1}{\Theta}\nabla P + \frac{1}{\Theta}\nabla \cdot \left[\frac{\Upsilon}{Re}(\nabla \vec{V} + \nabla \vec{V}^T)\right] + \vec{G} + \frac{1}{\Theta We} K \nabla \alpha \frac{\Theta}{0.5(\Theta_l + \Theta_g)}, \tag{3}$$

Volume fraction equation:

$$\frac{\partial \alpha}{\partial \tau} + \vec{V} \cdot \nabla \alpha = 0, \tag{4}$$

where α represents the volume fraction of liquid in the Volume of Fluid (VOF) method, which is 1 in the liquid phase and 0 in the gas phase, and it can used to calculate the density and viscosity of the mixture.

After a comparison with the original dimensional governing equation, the equivalent density is $\rho^* = \Theta$ and the equivalent viscosity is $\mu^* = \frac{\Upsilon}{Re}$; thus, the liquid and gas densities and the viscosity are ${\rho_l}^* = 1$, ${\rho_g}^* = \frac{\rho_g}{\rho_l}$, ${\mu_l}^* = \frac{1}{Re}$, and ${\mu_g}^* = \frac{\mu_g}{Re\mu_l}$, respectively.

The dimensionless surface tension is

$$\sigma^* = \frac{1}{We}. \tag{5a}$$

According to (1a) and (1b), the diameter of the mother droplet is $d_m = \frac{Re^2 {\mu_l}^2}{We\sigma\rho_l}$ and its impact velocity is $u_{m,0} = \frac{We\sigma}{Re\mu_l}$.

Thus, the dimensionless pressure and gravity can be rewritten as

$$P = \frac{pRe^2 {\mu_l}^2}{We^2\sigma^2\rho_l}, \tag{5b}$$

$$G = \frac{gRe^4 {\mu_l}^4}{We^3\sigma^3\rho_l}, \tag{5c}$$

respectively. The Ohnesorge number and Bond number are derived as $Oh = \sqrt{We}/Re$ and $Bo = 0.25G\,We$, respectively. Therefore, from the Reynolds and Weber numbers, the dimensionless surface tension, pressure, and gravity can all be obtained, as well as the Oh and Bo numbers.

A water droplet in the air is studied with the following properties: $\rho_g = 1.225$ kg/m^3, $\rho_l = 10^3$ kg/m^3, $\mu_g = 1.79 \times 10^{-5}$ Pa s, $\mu_l = 10^{-3}$ Pa s, $\sigma = 0.073$ N/m, in the range $Re = 10 \sim 1000$, $We = 1 \sim 100$, droplet size $d_m = 0.137 \sim 4.57$ mm, and size ratio $a_i = 0.5 \sim 3.0$.

C. Initial and boundary conditions

The father droplet is stationary at the equilibrium contact angle $\theta_{eq} = 150°$ on the superhydrophobic surface. The mother droplet is in contact with the father droplet from above with incoming downward velocity $u_{m,0}$ at the initial state. The dimensionless domain size is 6×6, the left ($r = 0$) is the axis-symmetric boundary condition, and the upper ($z = 6$) and the right ($r = 6$) are the free boundary conditions under dimensionless atmospheric pressure. Because the minimum actual droplet size is around 0.137 mm, which is much larger than the nano-scale, the macro-scale model is adopted and the non-slip boundary condition is applied at the bottom ($z = 0$) instead of the slip boundary condition. After a grid-sensitivity study, the grid size is set as 0.01 in the central region, where droplet spreading occurs, and as 0.02 outside the region.

D. Numerical methodology

The governing equations are discretized using the finite-volume method in ANSYS Fluent 14.0. The momentum equations are solved using the second-order upwind scheme, and the pressure and velocity are coupled with the PISO (Pressure implicit with splitting of operator) algorithm. The volume fraction of the liquid phase at the interface is calculated using the Geo-Reconstruct method. An implicit first-order scheme is adopted for time marching with a time step of 10^{-3}; the convergence criterion is that the residuals for the continuity equation and momentum equation at each time step are lower than 10^{-5}.

III. RESULTS AND DISCUSSION

A. Model validation

To prove the reliability of our numerical model, transient evolutions of droplet profiles in our numerical simulation results are compared with those of experimental observation.[8,18] Farhangi *et al.*[8] showed experimentally that a mother droplet collides with a father droplet of the same size on a superhydrophobic surface at an equilibrium contact angle of 156°. Zhang *et al.*[18] showed experimentally that when a mother droplet approaches a larger father droplet with negligible velocity, droplet coalescence is driven by surface capillarity. Transient evolutions of droplet profiles are provided in Fig. 2. The predicted profiles in our numerical model agree

Published under license by AIP Publishing

quite well with those from the experiment, proving that our numerical model is reliable.

B. Droplet collision regimes

Figure 3 shows the regimes for droplet collision in an *Oh*-*We* diagram, with the dimensionless parameters for typical cases in Table I. Clearly, droplet collision is affected by *We*, *Re*, *Oh*, and the droplet diameter ratio a_i. The whole region can be divided into three subregions according to the line of $We = 1$, $Oh = 1$, and $Re = 1$ ($We = Oh^2$). At high *We* numbers, the droplet collision is driven by the incoming droplet impact, and at low *We* numbers, it is driven by the capillary forces. Since the water droplet is studied with fixed properties, the *Oh* number reflects the droplet size variation. At a high *Oh*

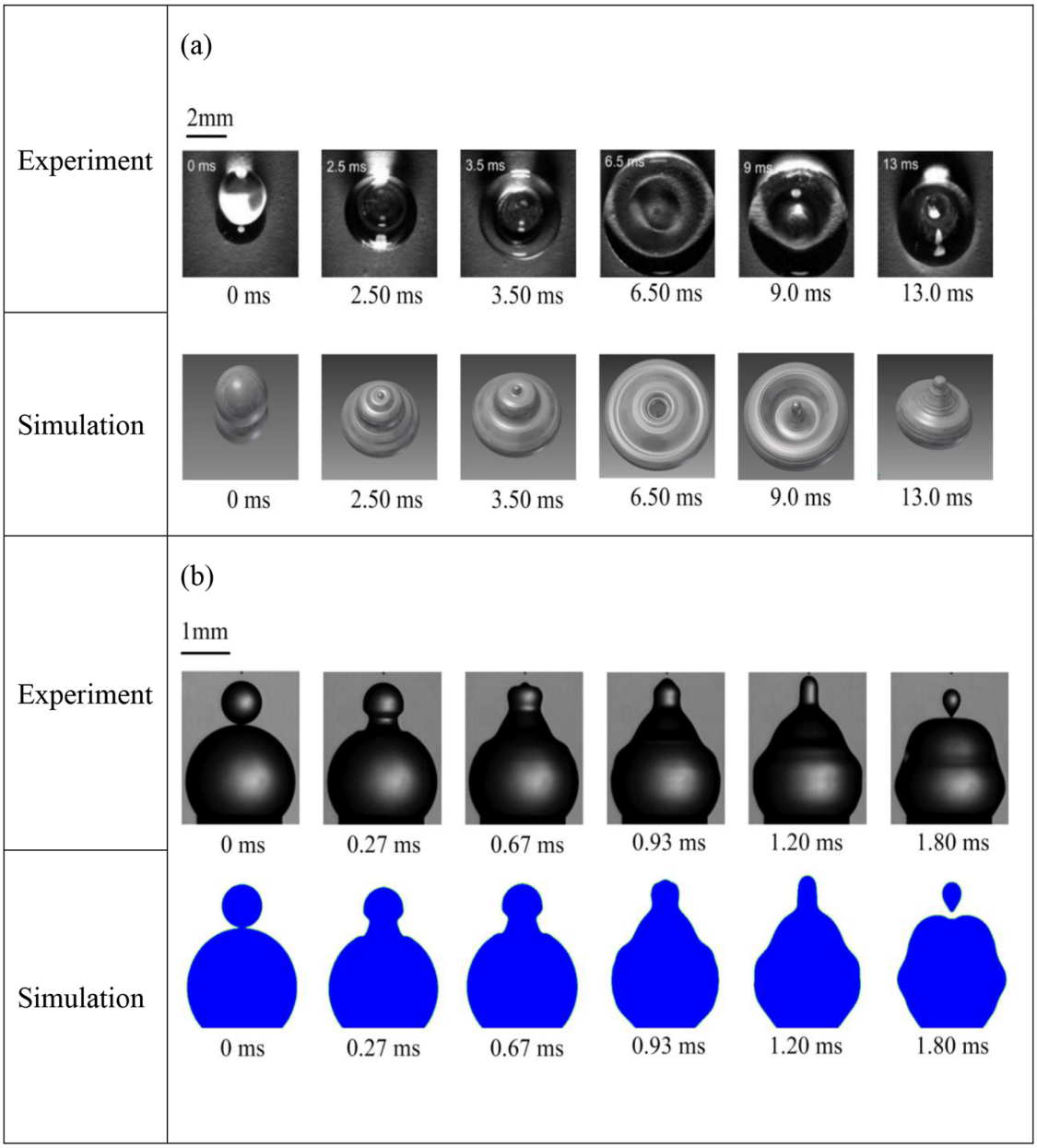

FIG. 2. Comparison of droplet profile evolution during droplet coalescence between our simulation and experimental results. (a) The droplet collision experiment by Farhangi *et al.*[8] ($d_m = d_f = 2.59$ mm, based on an impact velocity $u_0 = 0.744$ m/s, $Re = 2027$, and $We = 19.8$). (b) The capillary-driven droplet coalescence experiment by Zhang *et al.*[18] ($d_m = 0.60$ mm and $d_f = 1.63$ mm, based on a capillary-inertial velocity $u_0 = 0.349$ m/s, $Re = 209.3$, and $We = 1$).

Published under license by AIP Publishing

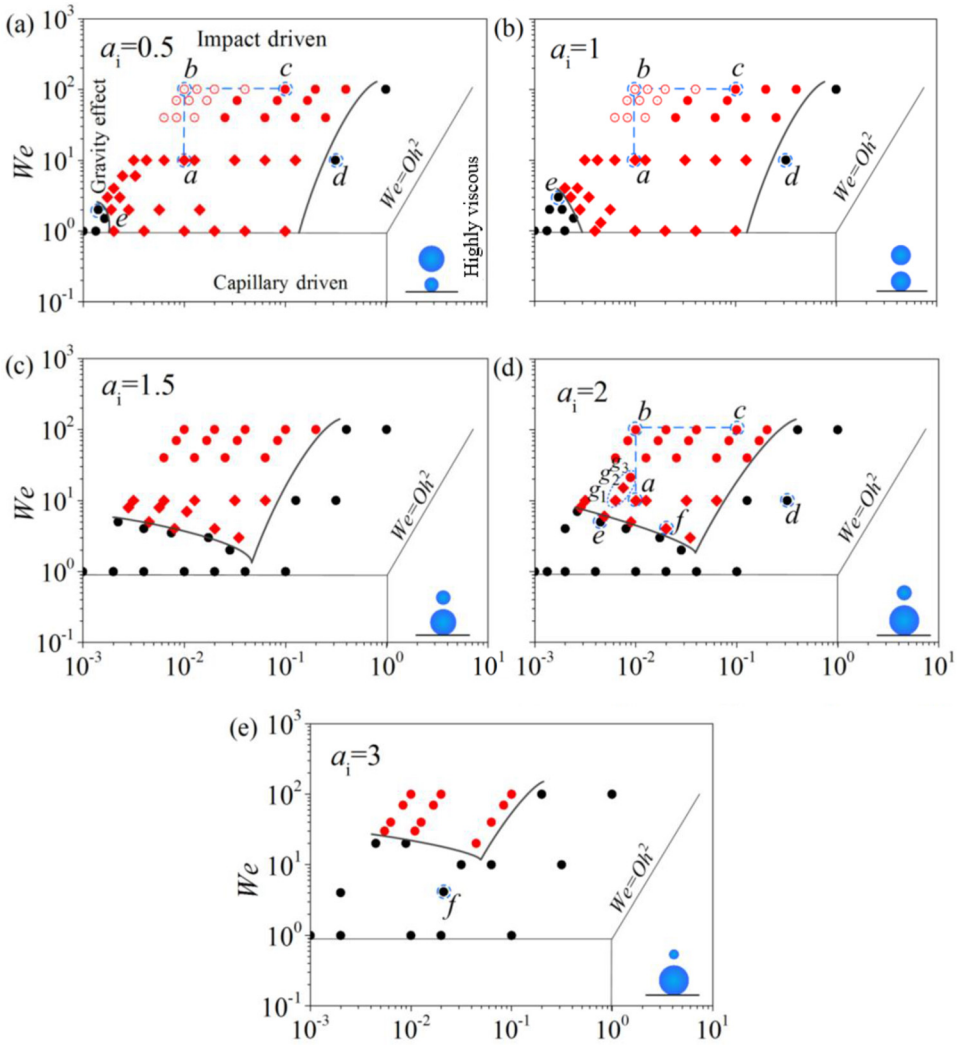

FIG. 3. Regimes for droplet collision for different size ratios of the father droplet to the mother droplet. (a) Size ratio $a_i = 0.5$. (b) Size ratio $a_i = 1.0$. (c) Size ratio $a_i = 1.5$. (d) Size ratio $a_i = 2.0$. (e) Size ratio $a_i = 3.0$. Corresponding values of *Oh* and *We* at different locations are as follows: a (0.01, 10); b (0.01, 100); *c* (0.1, 100); *d* (0.316, 10); *e* (1.73×10^{-3}, 3); f (0.02, 4); g_1 (1.73×10^{-3}, 10); g_2 (7.56×10^{-3}, 15); and g_3 (8.94×10^{-3}, 20).

TABLE I. Dimensionless parameters for typical cases in Fig. 3.

Case	*Re*	*We*		P_{atm}	*Oh*	*G*	*Bo*
a	316	10	0.10	190	0.01	2.52×10^{-4}	6.30×10^{-4}
b	1000	100	0.01	19	0.01	2.52×10^{-5}	6.30×10^{-4}
c	100	100	0.01	0.19	0.10	2.52×10^{-9}	6.30×10^{-8}
d	10	10	0.10	0.19	0.316	2.52×10^{-10}	6.30×10^{-10}
e	1000	3.0	0.33	2.11×10^{4}	1.73×10^{-3}	0.93	0.70
f	100	4.0	0.25	118.0	0.02	3.94×10^{-5}	3.94×10^{-5}
g_1	500	10	0.10	474	6.32×10^{-3}	1.58×10^{-3}	3.94×10^{-3}
g_2	500	15	0.067	211	7.75×10^{-3}	4.67×10^{-4}	1.75×10^{-3}
g_3	500	20	0.05	118	8.94×10^{-3}	1.97×10^{-5}	9.85×10^{-4}

Published under license by AIP Publishing

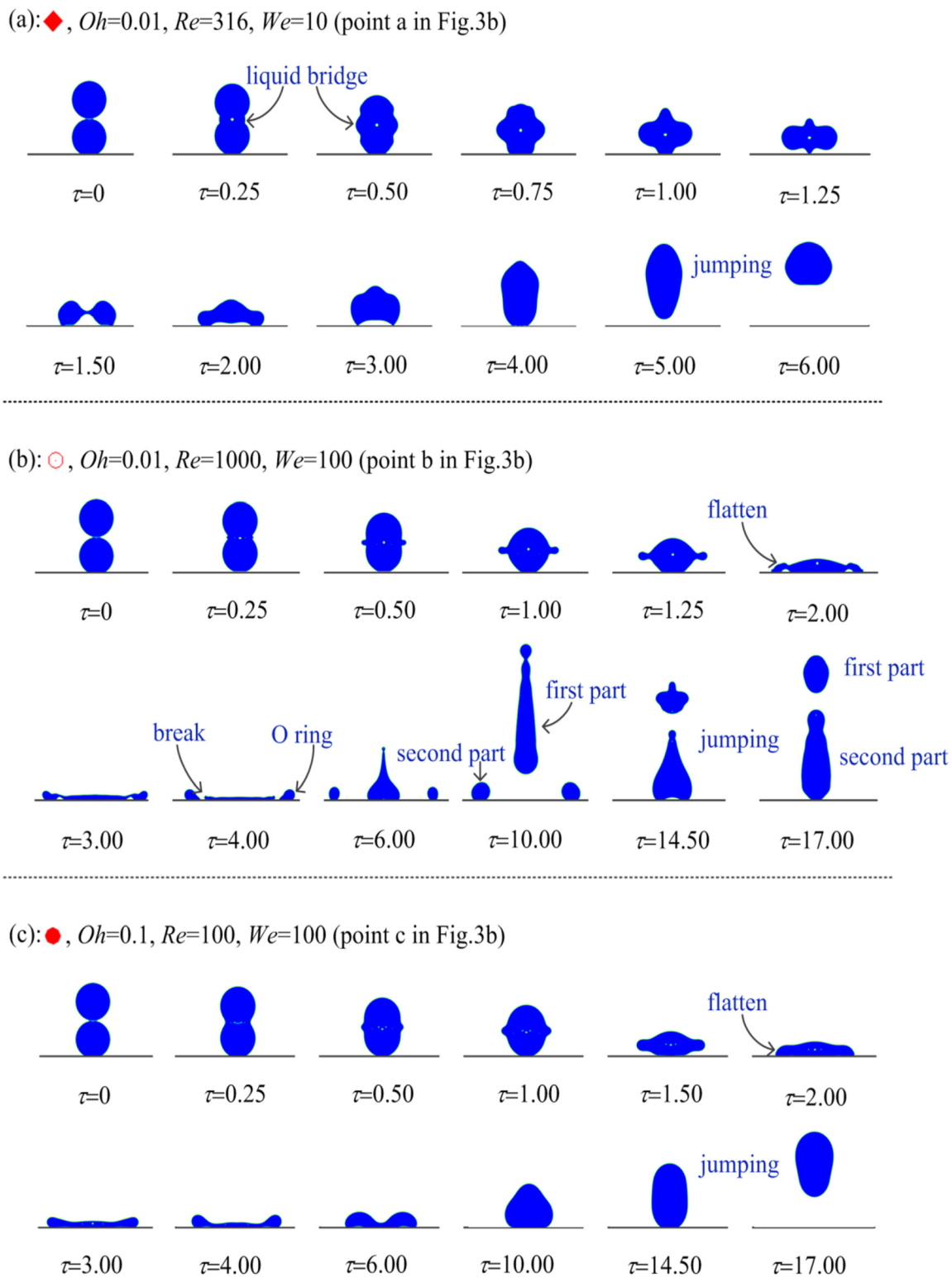

FIG. 4. Snapshots of droplet profiles with equal sizes: (a) $Oh = 0.01$, $We = 10$, and $Re = 316$, liquid bridge forming and bouncing back. (b) $Oh = 0.01$, $We = 100$, and $Re = 1000$, droplet flattening and jumping up with breakup. (c) $Oh = 0.1$, $We = 100$, and $Re = 100$, droplet flattening and jumping up without breakup.

Published under license by AIP Publishing

number, the droplet size is small; hence, the viscous effect is strong and the kinetic energy and surface energy can both be dissipated through viscous dissipation; hence, the merged droplet after collision cannot jump up. This is not the focus of our study, instead we will focus the region at $We \geq 1$ and $Re > 1$. This region can be divided into two sub-regions: the jumping regime (red symbols) and no-jumping regime (black symbols). For a droplet diameter ratio $a_i \leq 1$, a merged droplet can easily jump up after coalescence upon collision due to the large impact dynamics. The jumping region can further be divided into three sub-regions, depending on the *We* and *Oh* numbers: (1) For the mother droplet at a low *Oh* number or large size, the liquid bridges are formed during collision because the capillary force is relatively strong (the solid red diamonds around point a); (2) with the increasing impact dynamics at a high *We* number, the merged droplet will be flattened and break up without the formation of the liquid bridge (the hollow red circles around point b); (3) when the droplet size is decreased with increasing *Oh* number, the merged droplet will also flatten but will not break up (the solid red circles around point c).

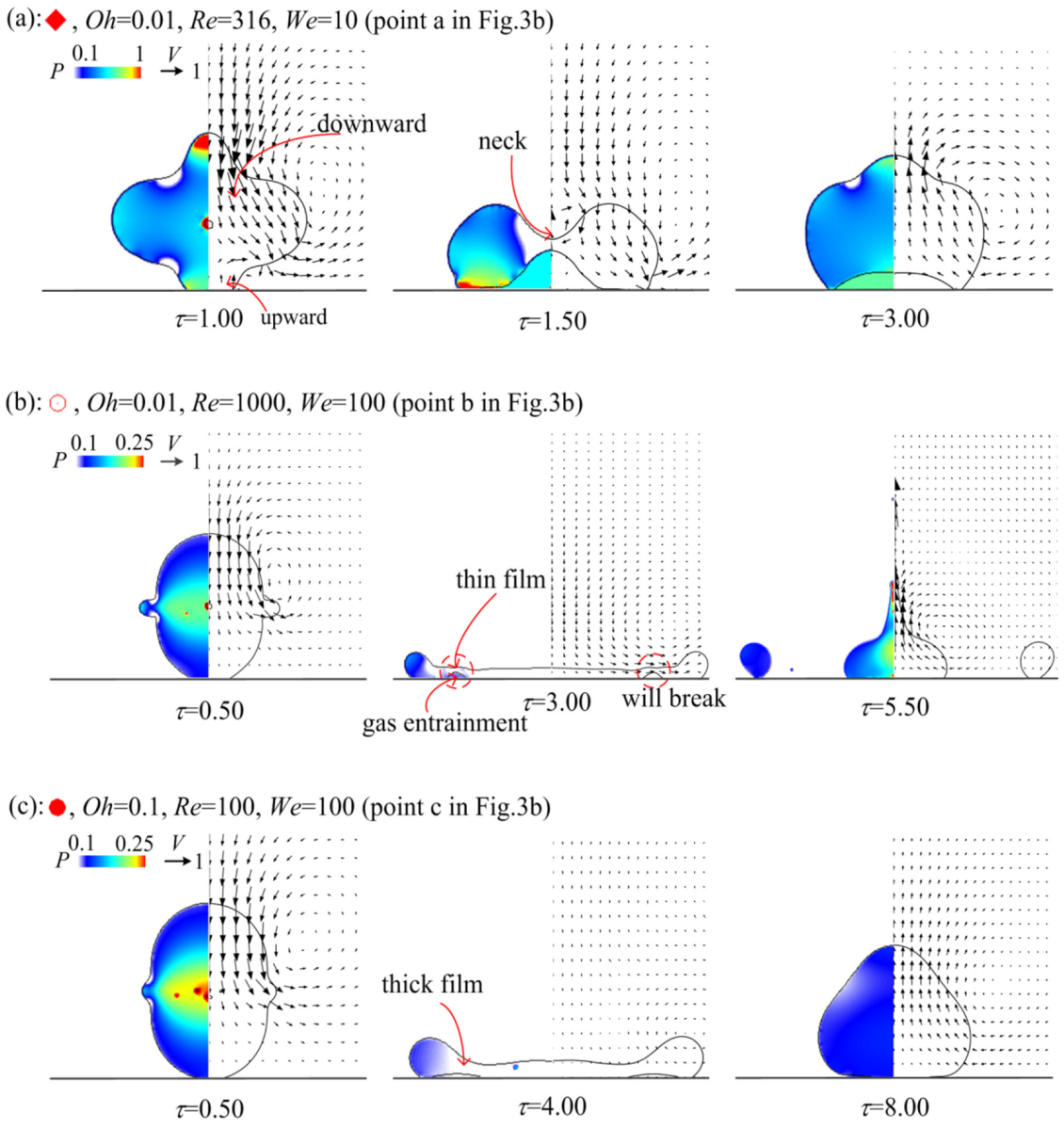

FIG. 5. Pressure and velocity fields for droplets of equal size with jumping (a) $Oh = 0.01$, $We = 10$, and $Re = 316$, liquid-bridge forming and bouncing back; (b) $Oh = 0.01$, $We = 100$, and $Re = 1000$, droplet flattening and jumping up with breakup; and (c) $Oh = 0.1$, $We = 100$, and $Re = 100$, droplet flattening and jumping up without breakup.

Published under license by AIP Publishing

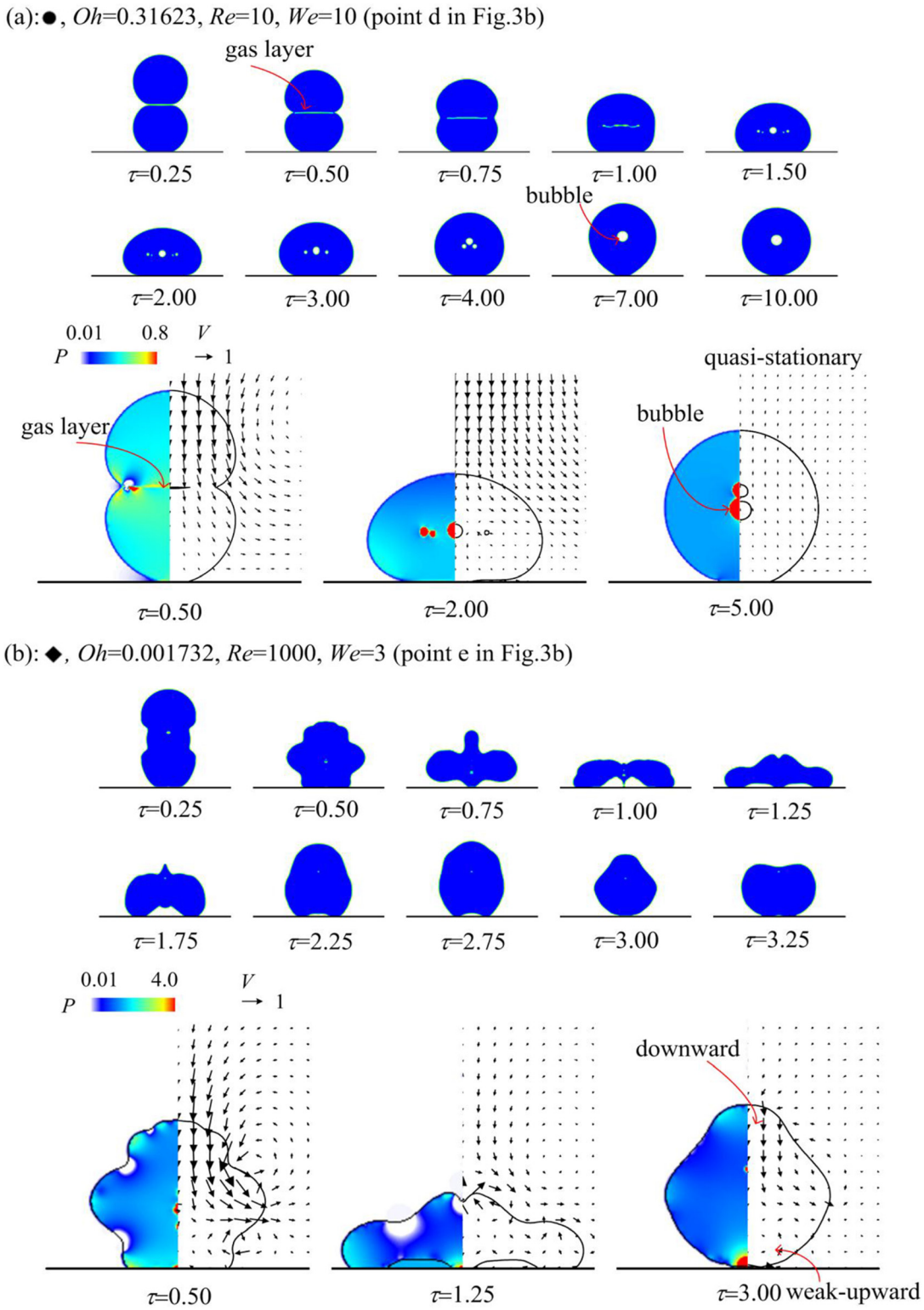

FIG. 6. Pressure and velocity fields for droplets of equal size without jumping. (a) No jumping due to high viscosity ($Oh = 0.316$, $We = 10$, and $Re = 10$). (b) No jumping due to high gravity ($Oh = 1.73 \times 10^{-3}$, $We = 3$, and $Re = 1000$).

Published under license by AIP Publishing

With increasing size ratio a_i, the jumping region is reduced. For $a_i > 1$, droplet breakup will not occur, and there are only two sub-regions: (1) a sub-region with liquid-bridge formation (the solid red diamond) and (2) a sub-region without liquid bridge formation (the solid red circles) in which the mother droplet merges with the father droplet.

C. Droplet collision with equal sizes

The dynamics of droplet collision are first investigated when both the father and mother droplets have the same size; the effects of *Re*, *We*, and the corresponding *Oh* numbers on droplet collision are examined for the ranges $Re = 10–1000$, $We = 1–100$, and $Oh = 0.001–1$.

1. Droplet collision dynamics

Figure 4 shows the evolution of droplet profiles during collision. For $Oh = 0.01$, $Re = 316$, and $We = 10$, at the initial stage of droplet collision, a liquid bridge is formed and prolonged when droplets are in contact with each other. Due to the large capillary force at low *We* numbers, the father droplet and mother droplet merge together. At $\tau = 1.0$, an upward velocity is generated at the bottom of the father droplet near the surface, as shown in Fig. 5(a), with a large downward velocity in the mother droplet. The merged droplet expands from the center in the horizontal direction, forming a neck at the center at $\tau = 1.5$. Due to the strong capillary force, the droplet retracts, eventually jumping up at $\tau = 5.0$.

When the *We* number is increased to 100, as shown in Fig. 4(b), inertial effects predominate compared with capillary and viscous effects. A liquid bridge is not obvious upon droplet collision. At $\tau = 0.5$, a skirt is formed upon strong collision of the mother droplet with the father droplet, and it will start to expand. In the meanwhile, the majority of the merged droplet will be flattened due to strong impact

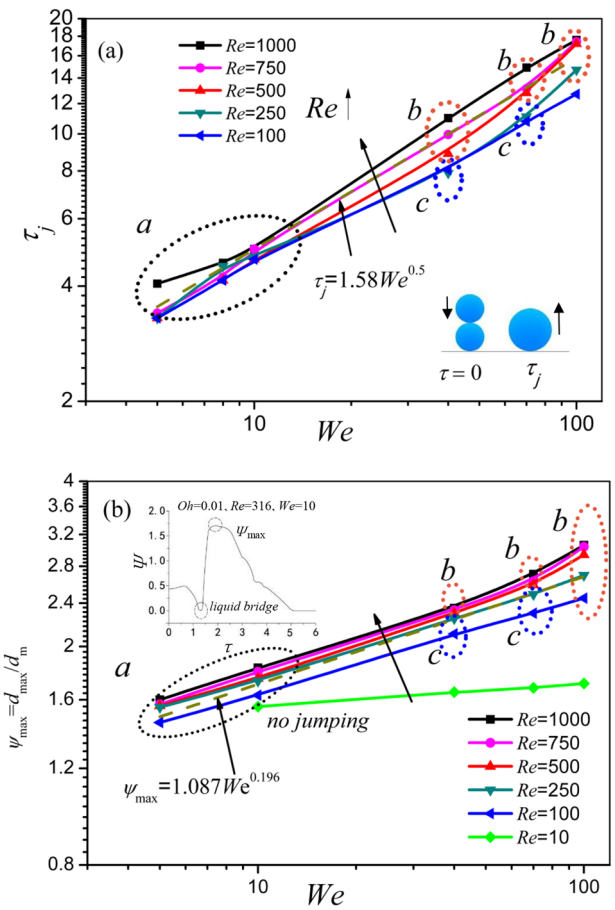

FIG. 7. Dependence of (a) contact time and (b) the maximum spreading diameter on the Weber number of equally sized droplet impacts.

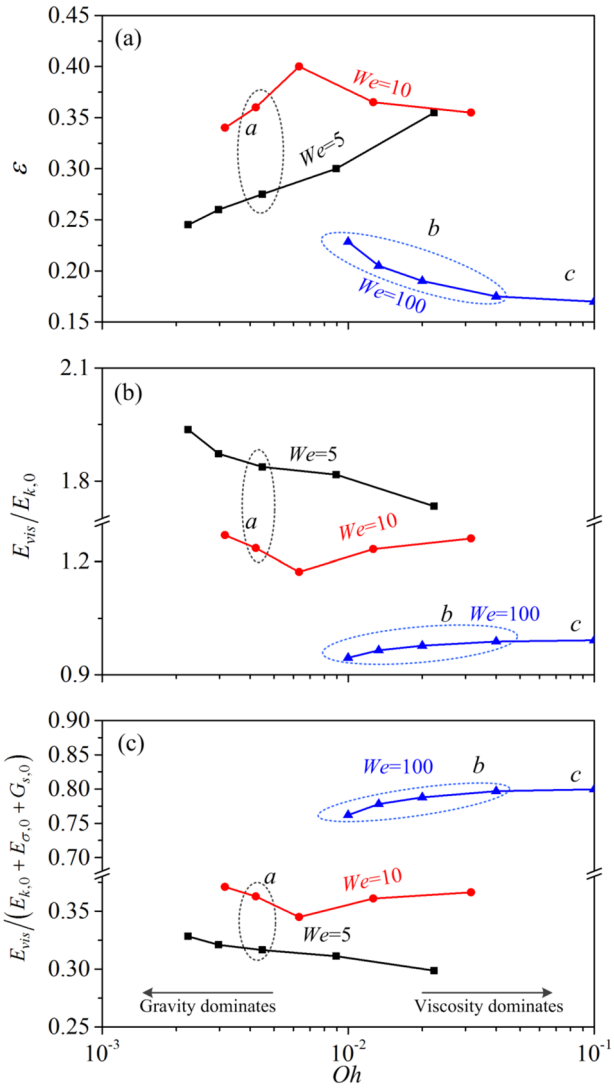

FIG. 8. Dependence of (a) the restitution coefficient, (b) the ratio of viscous dissipation to initial kinetics, and (c) the ratio of viscous dissipation to total energy on the *Oh* number for different Weber numbers for equally sized droplets.

Published under license by AIP Publishing

dynamics, and the gas pocket is trapped between the ring and the central region, and the thin film is formed connecting the tip and main body of the droplet, as shown in Fig. 5(b). Due to strong inertial effect, the thin film is not stable, and it will break up with O-ring formation. The remaining droplet retracts and jumps up as the jet, potentially forming a satellite droplet at the jet tip.

In Fig. 4(c), the *Oh* number increases to 0.1 at $We = 100$, indicating that viscosity plays a role in droplet dynamics. At the initial stage, it is similar to that at $Oh = 0.01$ in Fig. 4(b). However, after the merged droplet is flattened at the surface, as shown in Fig. 5(c), a thick film is formed without breakup at $\tau = 4.0$ due to a relatively large viscous effect. Under the capillary force, the flat droplet starts to retract, jumping up from the surface without breakup.

Figure 3 shows that the no-jumping regions are located on the left region and the right region. Taking point d in Fig. 3(b), for $Re = 10$ and $We = 10$, with a corresponding $Oh = 0.316$ as an example, viscous dissipation is related to the velocity gradient inside the droplet. Figure 6(a) shows that for large *Oh*, the impact dynamics are dissipated quickly by viscous dissipation. Due to the large viscosity, the mother and father droplets merge together, without a liquid bridge and bursting jet formation, forming a spherical cap on the substrate. At $\tau = 5.0$, the velocity inside the droplet becomes negligible, indicating that the impact kinetics are almost dissipated by the viscosity; hence, there is little energy for the droplet to rebound from the substrate. The effect of gravity is studied using point e in Fig. 3(b) as an example. Here, $Re = 1000$, $We = 3$, correspondingly, $Oh = 1.73 \times 10^{-3}$, and $Bo = 0.70$. Figure 6(b) shows that at the initial collision and spreading stage, gravity has little effect on droplet dynamics but plays a significant role in the retracting and rebounding stage. At $\tau = 3.0$, the droplet has not departed from the substrate, and the velocity at the top points downward. The velocity at the bottom is upward and is

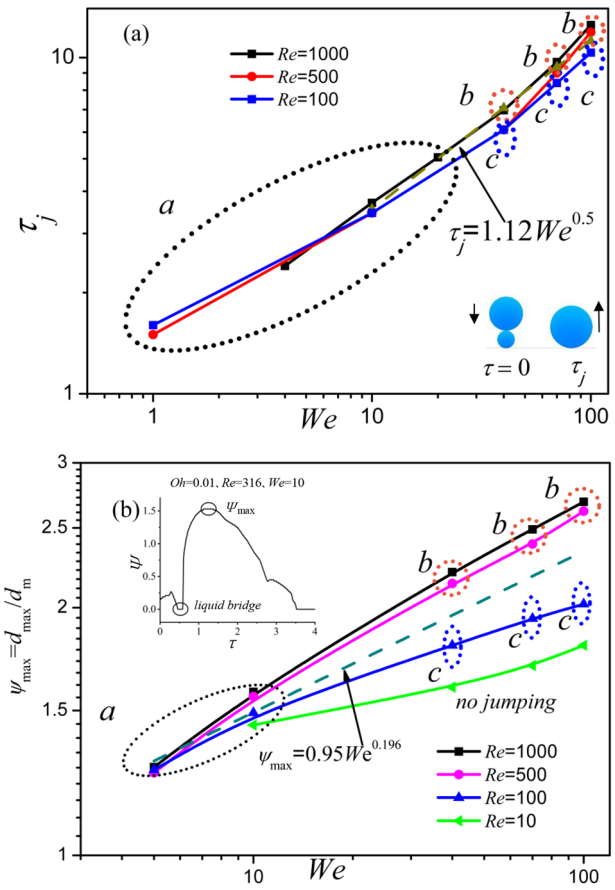

FIG. 9. Dependence of (a) contact time and (b) the maximum spreading diameter on the Weber number of unequally sized droplet impacts (size ratio of the lower droplet to the upper droplet $a_i = 0.5$).

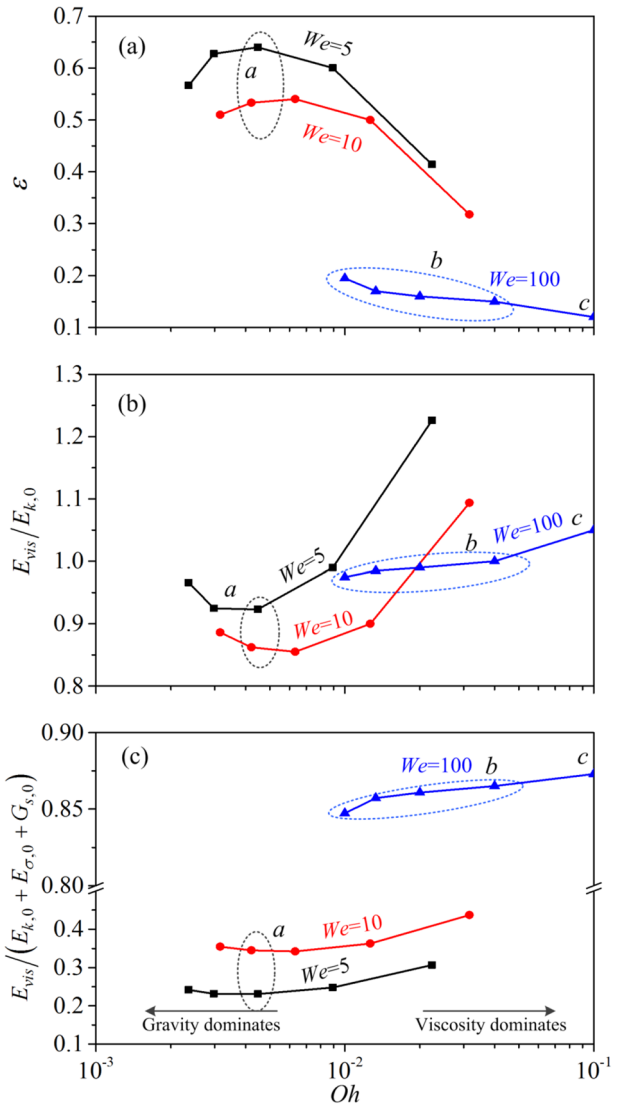

FIG. 10. Dependence of (a) the restitution coefficient, (b) the ratio of viscous dissipation to initial kinetics, and (c) the ratio of viscous dissipation to total energy on the *Oh* number for different Weber numbers for unequally sized droplets (size ratio of the lower droplet to the upper droplet $a_i = 0.5$).

Published under license by AIP Publishing

quite weak, preventing droplet departure from the substrate due to gravity.

2. Contact time and spreading diameter

The contact time and spreading diameter are crucial parameters in droplet collision on the surface. For a single droplet collision, Richard *et al.*[25] found that a droplet goes through flattening, retraction, and rebound stages. The deformation time between the droplet and surface is proportional to the capillary-inertial time $t_j \approx \left(\rho d_m^3/\sigma\right)^{1/2}$. This is confirmed by Graham *et al.*,[24] who showed that the contact time in droplet coalescence is related to the droplet diameter as $t_j \propto {d_m}^{1.5}$; thus, the dimensionless contact time is $\tau_j = t_j u_{m,0}/d_m \propto We^{0.5}$. After fitting with our data, $\tau_j = CWe^{0.5}$ is obtained, as shown in Fig. 7(a). Here, C is a coefficient dependent on the Reynolds number, which is 1.58 for $Re = 750$. When the Weber number is large, for large Re numbers, the droplet deforms easily due to large inertial effects and the contact time from impact to rebound is prolonged; hence, coefficient C increases, while for low Re numbers, coefficient C decreases. However, when the Weber number is small, droplet collision is mainly determined by surface tension, and the effect of the Reynolds number on droplet collision is negligible.

Graham *et al.*[24] showed that for a two-droplet impact, involving equally sized droplets, the maximum spreading diameter is proportional to $We^{0.2}$. After fitting with our data, $\psi_{max} = D\mathrm{We}^{0.196}$ is obtained; the power index is quite close to that of Graham *et al.*[24] The

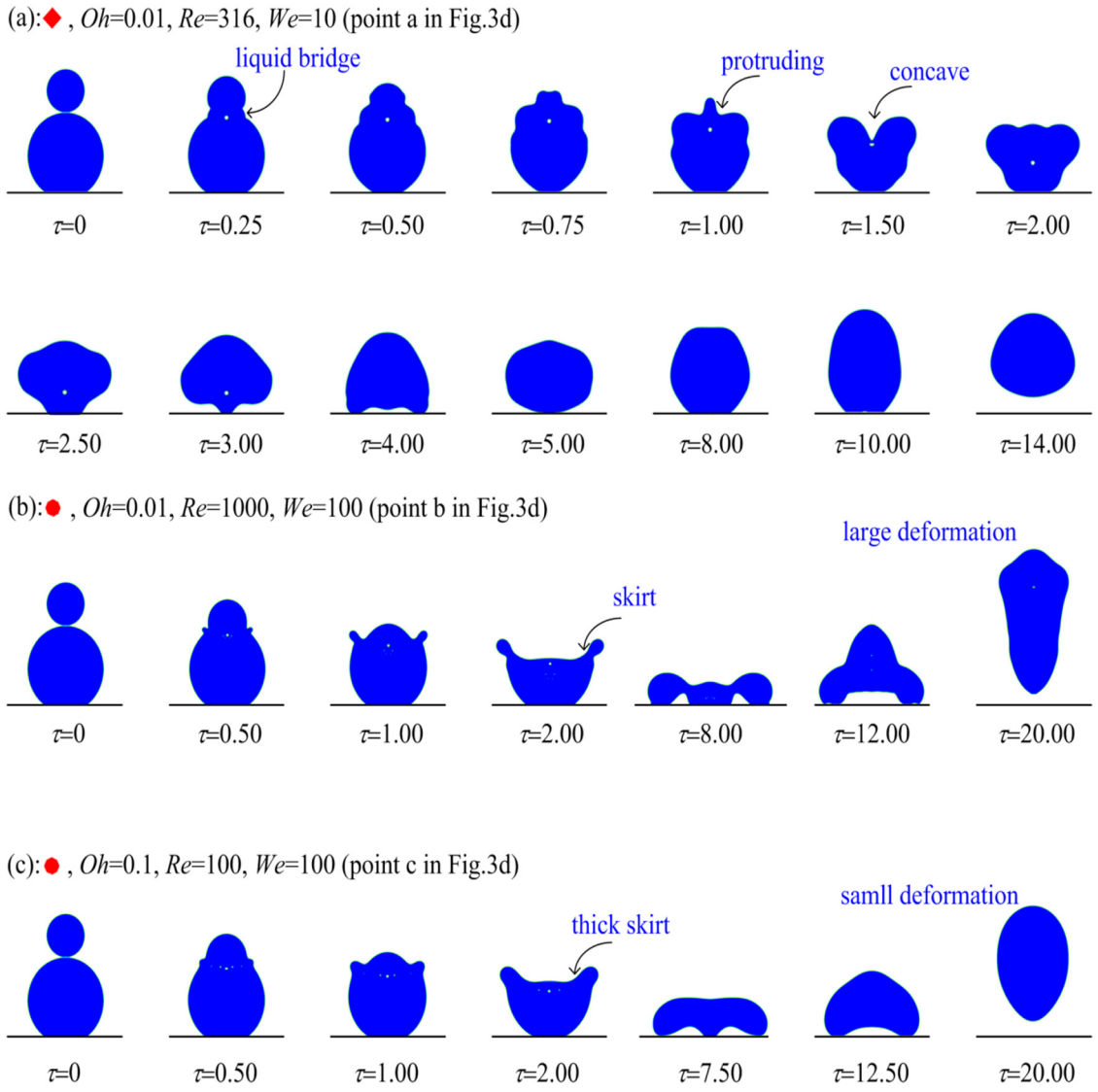

FIG. 11. Snapshots of droplet profiles during collision, with size ratio $a_i = 2.0$: (a) $Oh = 0.01$, $We = 10$, and $Re = 316$, liquid-bridge formation without bounce back; (b) $Oh = 0.01$, $We = 100$, and $Re = 1000$, coalescence and jumping up; and (c) $Oh = 0.1$, $We = 100$, and $Re = 100$, coalescence and jumping up.

Published under license by AIP Publishing

coefficient D is around 1.087 at $Re = 250$. Figure 7(b) clearly shows that with increasing We number, the maximum spreading diameter increases because the high impact kinetics at high We promote droplet spreading. The spreading radius of a single droplet increases monotonically when the droplet comes in contact with the substrate; but when one droplet impacts on another droplet on the substrate, the spreading differs significantly. Taking the case of $Oh = 0.01$, $Re = 316$, and $We = 10$ in Fig. 7(b) as an example, the droplet spreading radius first decreases, approaching zero, indicating that the merged droplet is capable of departing from the substrate; then, the spreading radius increases sharply to its maximum value and decreases again due to the droplet receding on the substrate.

At low We numbers, surface tension predominates during droplet impact, and the maximum spreading radius agrees well with the fitted correlation. However, at high We numbers, the effect of Re starts to play an important role. When Re is large, inertial effects predominate, and the impact kinetics are easily converted to spreading kinetics; this results in a large spreading radius; hence, the predicted spreading radius and coefficient D increases. At low Re numbers, due to strong viscous effects, the impact kinetics are dissipated by the viscous force and coefficient D decreases. At $Re = 10$, the merged droplet cannot jump up due to strong viscous dissipation.

3. Restitution coefficient and viscous loss

In order to examine the jumping dynamics after droplet impact, a restitution coefficient ϵ is used, which is defined as the outgoing velocity divided by the incoming velocity of the droplets. The outgoing velocity is calculated based on the volume averaged velocity of the detached droplet upon its departure from the droplet, and the incoming velocity is prescribed as 1 for the mother droplet.

Figure 8(a) shows that at low We, $We = 5$, and the droplet dynamics correspond to the left region in the We-Oh regime in Fig. 3, where gravity predominates. With increasing Oh, the corresponding Bo number decreases; hence, gravitational effects decrease, leading to a high restitution coefficient. If We is increased to 10, the restitution coefficient increases first to its maximum, then decreases with increasing Oh. For small Oh numbers, the corresponding Bo number is large and gravity predominates, while for large Oh numbers, viscous effects become predominant—both effects reduce the restitution coefficient. At medium Oh numbers, neither gravitational effects nor viscous effects predominate, and the restitution coefficient is at its maximum. If the We number is increased to 100, surface tension effects are weaker than inertial effects, and the drop dynamics are in the right region of the We-Oh regime, as shown in Fig. 3. In this region,

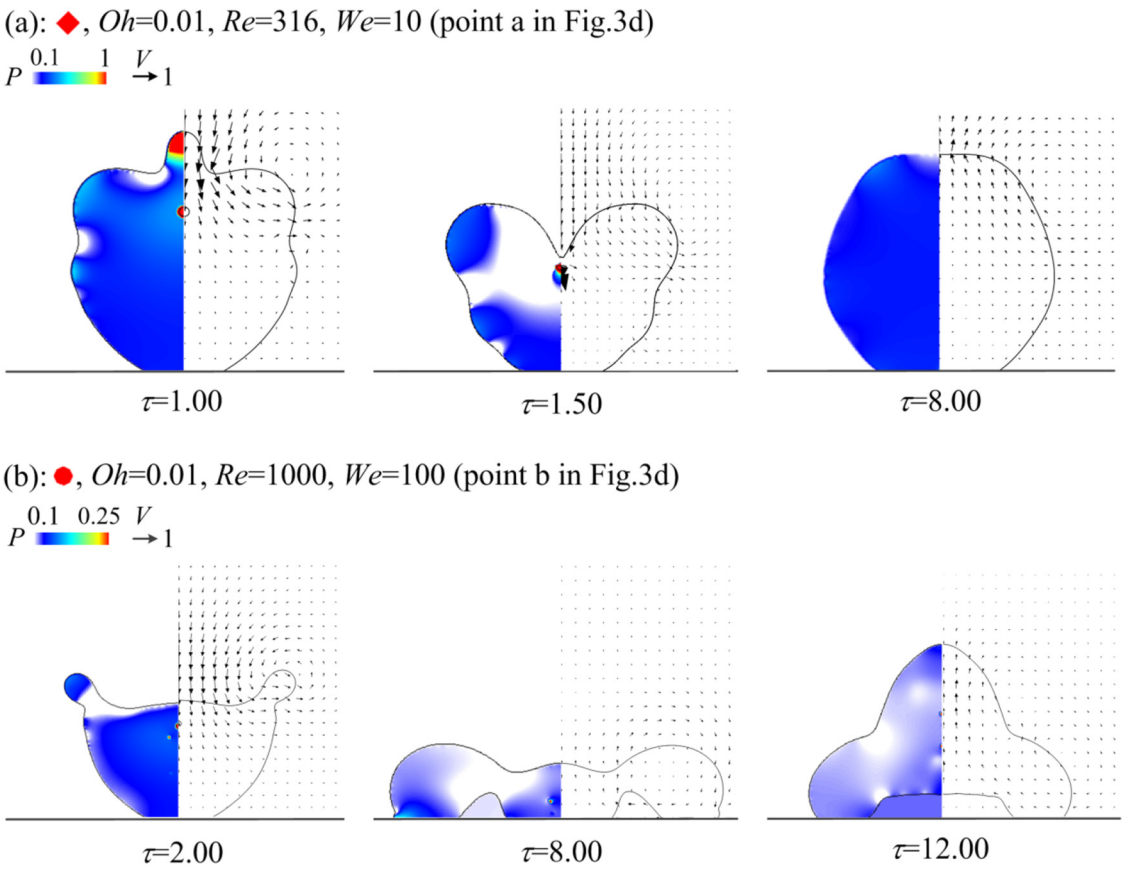

FIG. 12. Pressure and velocity fields for droplets with size ratio $a_i = 2.0$: (a) $Oh = 0.01$, $We = 10$, and $Re = 316$, liquid-bridge formation without bounce back; (b) $Oh = 0.01$, $We = 100$, and $Re = 1000$, coalescence and jumping up.

Published under license by AIP Publishing

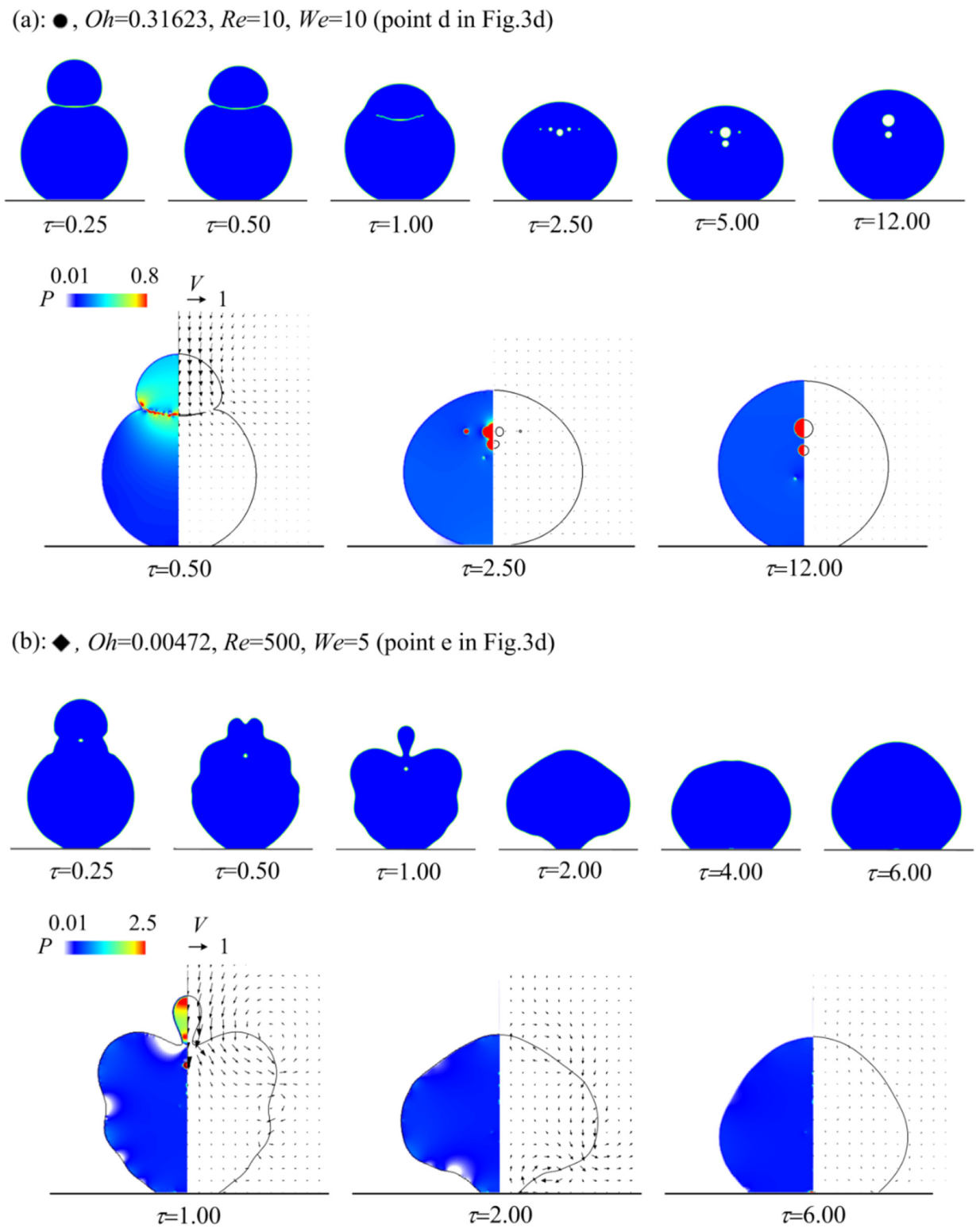

FIG. 13. Profiles, pressure, and velocity fields for droplets with size ratio $a_i = 2.0$ without jumping: (a) no jumping due to high viscosity ($Oh = 0.316$, $We = 10$, and $Re = 10$) and (b) no jumping due to large gravity ($Oh = 0.004\,72$, $We = 5$, and $Re = 500$).

Published under license by AIP Publishing

gravitational effects can be ignored, and a droplet goes through flattening, retraction, and jumping up stages. Figure 8(a) shows that the restitution coefficient decreases with increasing the *Oh* number; this is because increasing viscous effects dissipate increasing amounts of kinetic energy from the impact droplet.

In order to examine the effect of viscous dissipation during droplet impact, the viscous dissipation energy is calculated according to

$$E_{vis} = E_{k,0} + \Delta E_\sigma - E_h - E_{k,1}, \tag{6}$$

where $E_{k,0}$ is the kinetic energy of the incoming mother droplet, ΔE_σ is the released surface energy due to droplet impact, and E_h and $E_{k,1}$ are the gravitational potential energy and the kinetic energy of the merged droplet upon its departure from the substrate, respectively. All these values are obtained through numerical simulation. Figure 8(b) shows the ratio of the viscous dissipation energy to the initial kinetic energy. It is clear that the trend of the ratio contrasts with that of the restitution coefficient. For a given *We* number, high viscous dissipation leads to a low restitution coefficient. For low *We* numbers ($We \leq 10$), the viscous dissipation can be larger than the initial kinetic energy, indicating that the initial kinetic energy is not enough for the merged droplet to rebound; hence, the energy for rebounding should come from the released surface energy after coalescence of the mother droplet and the father droplet. Figure 8(c) shows the ratio of viscous dissipation energy to total initial energy for different *We* numbers. The total initial energy includes the initial impact kinetic energy of the mother droplets and the surface energy of both the mother and father droplets. The trend of the ratio is in contrast with that of the restitution coefficient. With increasing *We* number, inertial effects become predominant, leading to considerable deformation of the droplet; thus, viscous dissipation increases.

D. Droplet collision at low size ratio

Figure 3(a) shows that for a low size ratio of the father droplet to the mother droplet, i.e., when a large droplet impacts on a small droplet, the collision regime is quite similar to that for droplets of equal size; but the region for jumping up is larger, indicating that the merged droplet can easily jump up. After fitting with the data, Fig. 9 shows that the contact time is proportional to $We^{0.5}$ and that coefficient C decreases to 1.12 from 1.58 for an equally sized droplet collision. The maximum spreading diameter is still proportional to $We^{0.196}$, and coefficient D decreases to 0.95.

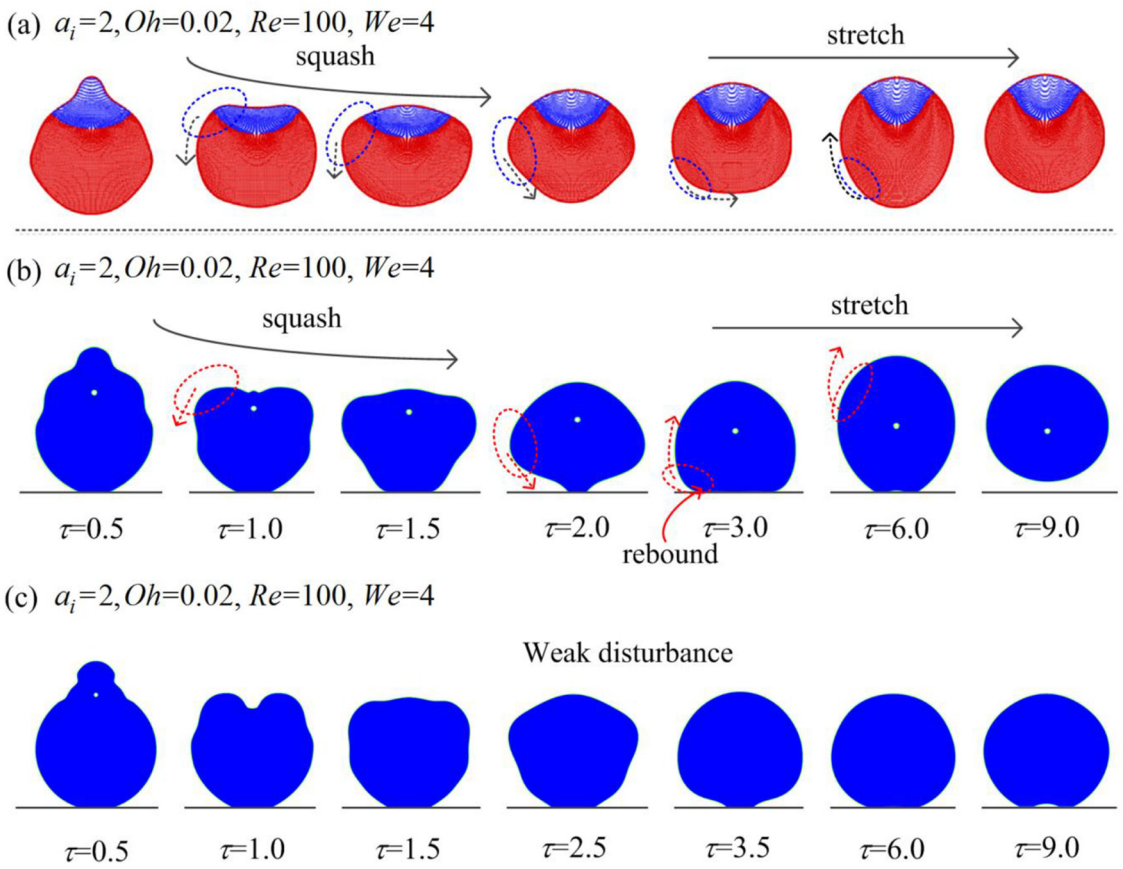

FIG. 14. Snapshots for droplet collision at low Weber number $We = 4$ for unequally sized droplets [point f in Fig. 3(d)]: (a) size ratio $a_i = 2.0$, coalescence in free air by Liu *et al.*;[23] (b) size ratio $a_i = 2.0$, coalescence upon impact with superhydrophobic substrate; and (c) size ratio $a_i = 3.0$, coalescence upon impact with superhydrophobic substrate.

Published under license by AIP Publishing

Figure 10 shows that at low *We* numbers, $We = 5$, with increasing *Oh*, the restitution coefficient first increases and then reaches its maximum value at around $Oh = 0.0045$ before it decreases; this trend is significantly different from the monotonical trend for an equally sized droplet collision. For a size ratio $a_i = 0.5$, at low *Oh* numbers, with correspondingly high *Bo* numbers, gravitational effects lessen; while at high *Oh* numbers, viscous effects start to play an important role, leading to a decreasing restitution coefficient. This is shown in Figs. 10(b) and 10(c): At low *We* numbers, the portions of viscous dissipation energy over both the initial kinetic energy and the initial total energy increase when the *Oh* number is larger than 0.0045.

E. Droplet collision at high size ratio

1. Jumping regime

For a large size ratio of the father droplet to the mother droplet, i.e., when a small droplet impacts on a large droplet, the no-jumping region in the collision regime becomes large because the initial impact kinetic energy is relatively low. Figure 11 shows the droplet collision and jump dynamics for a size ratio $a_i = 2.0$. At low *We* numbers ($We \leq 10$), surface tension is predominant, and upon contact between a mother droplet and a father droplet, a liquid bridge is formed. The mother droplet is pulled into the father droplet under surface tension at $\tau = 0.50$, and a large, merged droplet is formed. During coalescence, a capillary wave is formed and begins to propagate downward along the droplet surface. Figure 12(a) shows that at $\tau = 1.0$, high pressure and low pressure alternate along the crests and troughs of the capillary waves. After reaching the substrate, the capillary wave bounces back, causing the droplet to jump up. If the *We* number is increased to 100, surface tension weakens, while droplet inertia increases; thus, the droplet easily deforms during coalescence, as shown in Fig. 11(b), and a skirt forms upon contact at $\tau = 2.0$. Due to large downward impact kinetics, the edges of the merged droplet touch the substrate. From Fig. 12(b), it can be seen that the high pressure and upward velocity are generated at the bottom of the father droplet at $\tau = 8.0$, then the merged droplet starts to retract and jump up from the substrate. If the *Oh* number is increased to 0.1 at $We = 100$, due to viscous effects, the skirt at the edge becomes thicker, and after touching the substrate, the merged droplet rebounds with little deformation.

2. No-jumping regime

If the *Oh* number is large enough [e.g., 0.316, as shown in Fig. 13(a)], due to high viscous dissipation, a liquid bridge cannot be formed when the mother droplet impacts on the father droplet, but several tiny bubbles become trapped between the droplets. Although the mother droplet kinetics are quite large at $\tau = 0.50$, they dissipate quickly, and the velocity inside the merged droplet is negligible at $\tau = 2.50$.

If the *Bo* number is large enough, as shown in Fig. 13(b), strong capillary waves are generated due to high surface tension at low *We* numbers. A jet is generated when the waves reach the top, before being retracted to the merged droplet. When waves propagate to the bottom, they push the merged droplet from the substrate; however, due to gravity, the droplet cannot depart from the substrate and settle quickly.

During the head-on impact of a mother droplet and a father droplet, the substrate plays an important role. Because of the interaction between the droplet and the substrate, the downward kinetics of the mother droplet are converted into the upward kinetics of the merged droplet. Figure 14(a) shows the droplet dynamics for a size ratio $a_i = 2.0$ when there is no substrate, and a capillary wave can be generated upon the impact of the mother droplet on the suspended father droplet, propagating to the bottom before rebounding and traveling upward. Thus, the capillary wave travels downward and upward alternately, meaning that the merged droplet oscillates, coming to rest when the energy of the capillary wave is dissipated. However, in our study of droplet impact on a substrate, when the capillary wave reaches the substrate, it rebounds and travels upward, meaning that the merged droplet can depart from the substrate surface. If the size ratio a_i is increased to 3, i.e., the incoming mother droplet is much smaller than the father droplet, the impact kinetic energy is reduced and the capillary wave is weaker; the merged droplet, therefore, does not have enough energy to depart from the substrate.

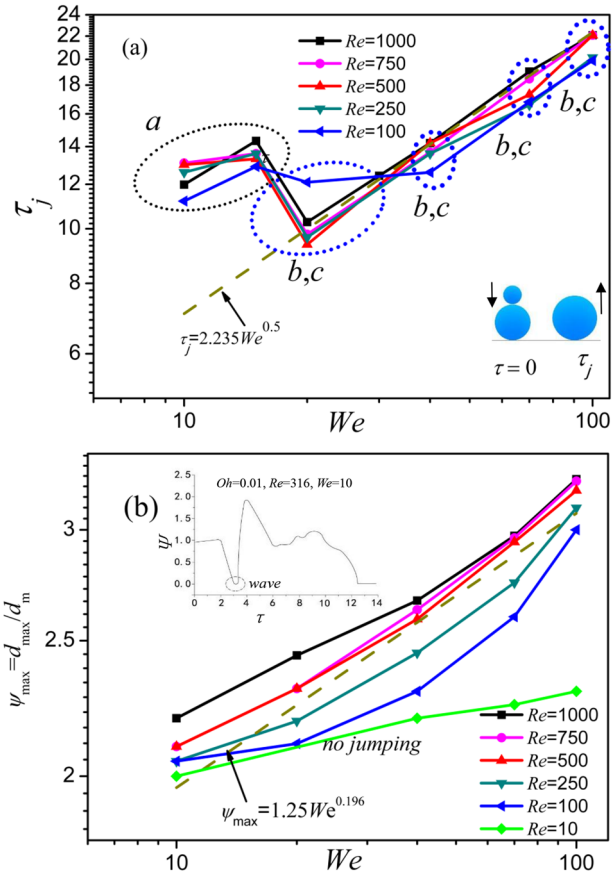

FIG. 15. Dependence of (a) contact time and (b) the maximum spreading diameter on the Weber number of unequally sized droplet impacts (size ratio of the lower droplet to the upper droplet $a_i = 2.0$).

Published under license by AIP Publishing

3. Contact time and spreading diameter

In Fig. 15(a), the contact time of the merged droplet with the substrate is fitted with the *We* number. When $We \geq 20$, the contact time is proportional to $We^{0.5}$, and the power law is similar to that when the mother droplet is equal to or larger than the father droplet. The only difference is that coefficient *C* increases (2.235). However, for $We \leq 15$, the contact time is very high because at low *We* numbers, the corresponding *Bo* numbers increase, indicating that gravitational effects become significant. Figure 16 shows that at low *We* numbers, when the capillary wave is rebounded by the substrate and travels to the top of the merged droplet at $\tau = 9.0$ for $We = 10$ and $\tau = 10.0$ for $We = 15$, the droplet cannot detach from the substrate due to gravity. In contrast, at $We = 20$, the merged droplet can detach from the substrate. Therefore, the contact time of the droplet at low *We* numbers will be much longer than that at high *We* numbers, meaning that the fitted correlation cannot be applied.

In Fig. 15(b), the maximum spreading diameter divided by the *We* number is fitted as $\psi_{max} = 1.25We^{0.196}$ for $Re = 250$; hence, the power law still holds independently of the droplet-size ratio. The maximum spreading diameter increases at high *Re* numbers due to more pronounced inertial effects, while at low *Re* numbers, it decreases because viscous effects start to affect drop impact. At $Re = 10$, the maximum spreading diameter is reduced significantly because the merged droplet cannot jump up due to very strong viscous effects. Notably, at $Oh = 0.01$, $Re = 316$, and $We = 10$, the spreading diameter becomes zero at around $\tau = 3.2$, but this does not mean that the merged droplet has jumped up from the substrate. Figure 11(a) shows that when a capillary wave travels downward to the substrate, the edges of the merged droplet touch the surface, while the bottom-center of the droplet rebounds from the substrate, leading to an almost-zero spreading diameter at this time instant.

Although the maximum spreading diameter follows the same scaling law as $We^{0.196}$, the coefficient *D* increases from 0.95 at the size ratio $a_i = 0.5$ to 1.25 at the size ratio $a_i = 2.0$. Because in our study, the mother droplet diameter is taken as the characteristic length, at low size ratio $a_i = 0.5$, the diameter of father droplet is low; thus, the overall volume of merged droplet is low, leading to a low maximum spreading diameter. On the contrary, at a large size ratio $a_i = 2.0$, the maximum spreading diameter becomes large.

4. Restitution coefficient and viscous dissipation

Figure 17(a) shows the variation in the restitution coefficient over the *Oh* number. At $We = 10$, the restitution coefficient first increases with increasing *Oh* number because at low *Oh* numbers, the corresponding *Bo* numbers are large, meaning that gravitational effects decrease. However, after reaching its maximum value, the restitution coefficient starts to decrease because viscous effects increase at high *Oh* numbers. At $We = 100$, surface tension and gravitational effects become weak, meaning that the droplet can easily deform; the restitution coefficient decreases with increasing *Oh* number because viscous effects increase.

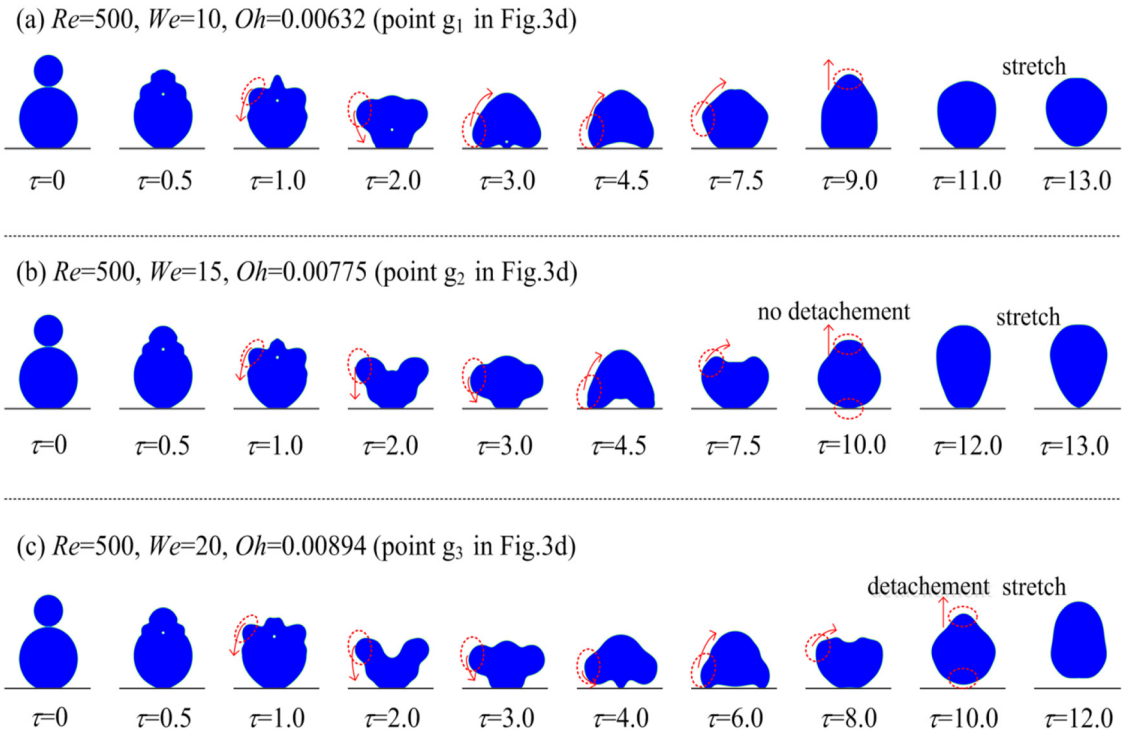

FIG. 16. Snapshots of droplet profiles during collision: (a) No jumping up after coalescence, $Re = 500$, $We = 10$, and $Oh = 0.00632$. (b) No jumping up after coalescence, $Re = 500$, $We = 15$, and $Oh = 0.00775$. (c) Jumping up after coalescence, $Re = 500$, $We = 20$, and $Oh = 0.008\,94$.

Published under license by AIP Publishing

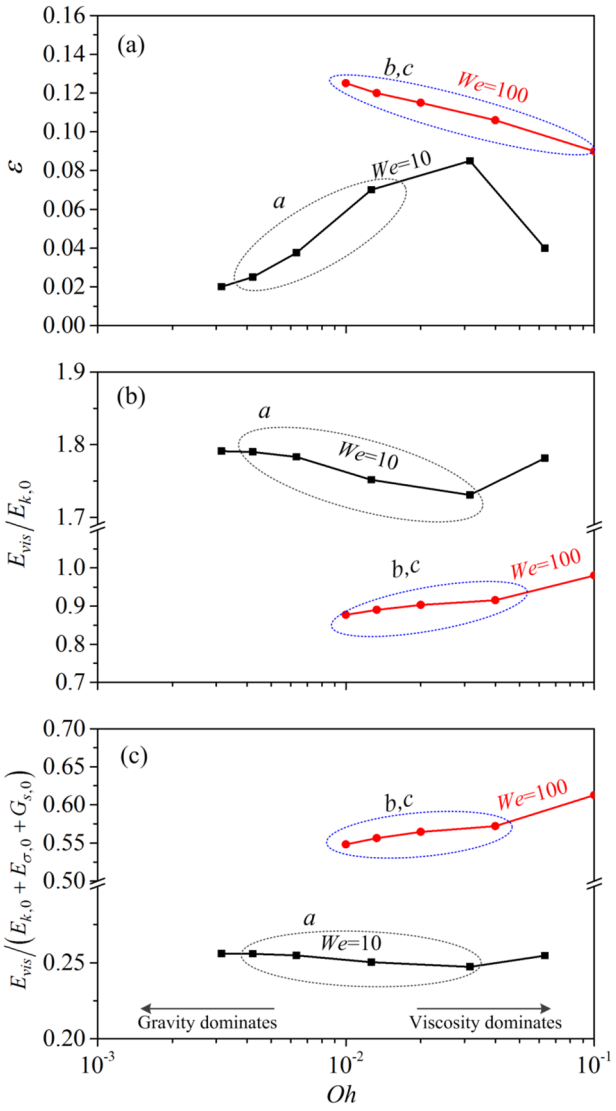

FIG. 17. Dependence of (a) the restitution coefficient, (b) the ratio of viscous dissipation to initial kinetics, and (c) the ratio of viscous dissipation to total energy on the *Oh* number for different Weber numbers for unequal droplet sizes $a_i = 2.0$.

Figures 17(b) and 17(c) show the variation in viscous dissipation over the initial kinetic energy and initial total energy. The variation in viscous dissipation is in contrast with the restitution coefficient. Energy is dissipated mainly through viscous effects, and a large restitution coefficient means that viscous dissipation is low. Interestingly, at $We = 100$, the ratio of viscous dissipation to total energy is much larger than that at $We = 10$; this is because at large *We* numbers, the droplet can easily deform due to low surface tension, meaning that viscous dissipation increases.

IV. CONCLUSION

In our study, a numerical simulation is carried out for the head-on impact of two droplets with different sizes on a superhydrophobic surface. A 2D axisymmetric model using the volume-of-fluid method simulates droplet evolution during impact, and jumping regimes are obtained for different dimensionless parameters. The main conclusions are summarized as follows:

(1) When a large droplet impacts on a small droplet, the merged droplet can easily jump up from the substrate due to large impact dynamics. The dynamics for droplet jumping mainly originate from the released surface energy after coalescence of the mother droplet and father droplet. At low *Oh* numbers, the corresponding *Bo* numbers are large, and the merged droplet cannot jump up due to significant gravitational effects; additionally, the merged droplet cannot jump up at high *Oh* numbers due to significant viscous effects.
(2) When a small droplet impacts on a large droplet, the jumping region in the collision regime is reduced due to the low impact dynamics. Capillary waves play an important role in the dynamics of the merged droplet. At low *We* numbers, the weak capillary wave cannot cause the droplet to jump up from the substrate due to significant gravitational or viscous effects.
(3) In head-on droplet collisions, the contact time of the merged droplet in contact with the substrate is proportional to $We^{0.5}$, and its maximum spreading diameter is proportional to $We^{0.2}$. With an increasing size ratio of the father droplet to the mother droplet, both the contact time and maximum spreading diameter increase.

ACKNOWLEDGMENTS

The research was supported by the Natural Science Foundation of China (Grant Nos. 51776064 and 52076077) and the Fundamental Research Funds for the Central Universities of China (Grant Nos. 2018ZD02 and 2020DF002).

DATA AVAILABILITY

The data that support the findings of this study are available from the corresponding author upon reasonable request.

REFERENCES

[1]D. M. Whelpdale and R. List, "The coalescence process in raindrop growth," J. Geophys. Res. **76**(12), 2836–2856, https://doi.org/10.1029/jc076i012p02836 (1971).
[2]R. Gunn, "Collision characteristics of freely falling water drops," Science **150** (3697), 695–701 (1965).
[3]X. D. Cheng, Y. L. Zhu, L. Zhang, D. Y. Zhang, and T. Ku, "Numerical analysis of deposition frequency for successive droplets coalescence dynamics," Phys. Fluids **30**, 042102 (2018).
[4]G. Finotello, J. T. Padding, N. G. Deen, A. Jongsma, F. Innings, and J. A. M. Kuipers, "Effect of viscosity on droplet-droplet collisional interaction," Phys. Fluids **29**(6), 067102 (2017).
[5]H. C. Cong, L. J. Qian, Y. T. Wang, and J. Z. Lin, "Numerical simulation of the collision behaviors of binary unequal-sized droplets at high Weber number," Phys. Fluids **32**, 103307 (2020).
[6]Z. Y. Zhang and P. Zhang, "Kinetic energy recovery and interface hysteresis of bouncing droplets after inelastic head-on collision," Phys. Fluids **29**, 103306 (2017).
[7]Q. Liu and M. Orme, "High precision solder droplet printing technology and the state-of-the-art," J. Mater. Process. Technol. **115**(3), 271–283 (2001).
[8]M. M. Farhangi, P. J. Graham, N. R. Choudhury, and A. Dolatabadi, "Induced detachment of coalescing droplets on superhydrophobic surfaces," Langmuir **28**(2), 1290–1303 (2012).

Published under license by AIP Publishing

[9]H. Mertaniemi, R. Forchheimer, O. Ikkala, and R. H. A. Ras, "Rebounding droplet-droplet collisions on superhydrophobic surfaces: From the phenomenon to droplet logic," Adv. Mater. **24**(42), 5738–5743 (2012).
[10]Y. J. Jiang, A. Umemura, and C. K. Law, "An experimental investigation on the collision behaviour of hydrocarbon droplets," J. Fluid Mech. **234**, 171–190 (1992).
[11]J. Qian and C. K. Law, "Regimes of coalescence and separation in droplet collision," J. Fluid Mech. **331**, 59–80 (1997).
[12]K. D. Willis and M. E. Orme, "Experiments on the dynamics of droplet collisions in a vacuum," Exp. Fluids **29**(4), 347–358 (2000).
[13]F.-C. Wang, J.-T. Feng, and Y.-P. Zhao, "The head-on colliding process of binary liquid droplets at low velocity: High-speed photography experiments and modeling," J. Colloid Interface Sci. **326**(1), 196–200 (2008).
[14]P. R. Brazier-Smith, S. G. Jennings, and J. Latham, "The interaction of falling water drops: Coalescence," Proc. R. Soc. A **326**(1566), 393–408 (1972).
[15]N. Ashgriz and J. Y. Poo, "Coalescence and separation in binary collisions of liquid drops," J. Fluid Mech. **221**, 183–204 (2006).
[16]C. Rabe, J. Malet, and F. Feuillebois, "Experimental investigation of water droplet binary collisions and description of outcomes with a symmetric Weber number," Phys. Fluids **22**(4), 047101 (2010).
[17]C. Tang, P. Zhang, and C. K. Law, "Bouncing, coalescence, and separation in head-on collision of unequal-size droplets," Phys. Fluids **24**(2), 022101 (2012).
[18]F. H. Zhang, E. Q. Li, and S. T. Thoroddsen, "Satellite formation during coalescence of unequal size drops," Phys. Rev. Lett. **102**(10), 104502 (2009).
[19]N. Yi, B. Huang, L. Dong, X. Quan, F. Hong, P. Tao, C. Y. Song, W. Shang, and T. Deng, "Temperature-induced coalescence of colliding binary droplets on superhydrophobic surface," Sci. Rep. **4**(6175), 4303 (2014).
[20]B. Sakakibara and T. Inamuro, "Lattice Boltzmann simulation of collision dynamics of two unequal-size droplets," Int. J. Heat Mass Transfer **51**(11-12), 3207–3216 (2008).
[21]K. N. Premnath and J. Abraham, "Simulations of binary drop collisions with a multiple-relaxation-time lattice-Boltzmann model," Phys. Fluids **17**(12), 122105 (2005).
[22]N. Nikolopoulos and G. Bergeles, "The effect of gas and liquid properties and droplet size ratio on the central collision between two unequal-size droplets in the reflexive regime," Int. J. Heat Mass Transfer **54**, 678–691 (2011).
[23]D. Liu, P. Zhang, C. K. Law, and Y. C. Guo, "Collision dynamics and mixing of unequal-size droplets," Int. J. Heat Mass Transfer **57**, 421–428 (2013).
[24]P. J. Graham, M. M. Farhangi, and A. Dolatabadi, "Dynamics of droplet coalescence in response to increasing hydrophobicity," Phys. Fluids **24**(11), 112105 (2012).
[25]D. Richard, C. Clanet, and D. Quéré, "Contact time of a bouncing drop," Nature **417**, 811 (2002).

Published under license by AIP Publishing